ACCOUNTS
of chemical research

Biological Water Oxidation

NICHOLAS COX,* DIMITRIOS A. PANTAZIS, FRANK NEESE, AND WOLFGANG LUBITZ*

Max Planck Institute for Chemical Energy Conversion, Stiftstrasse 34-36, D-45470 Mülheim an der Ruhr, Germany

RECEIVED ON DECEMBER 6, 2012

CONSPECTUS

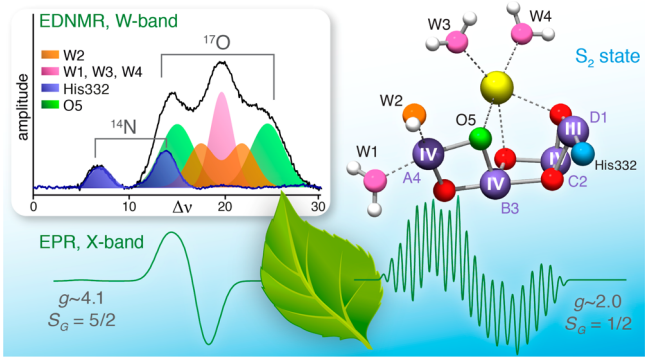

Photosystem II (PSII), a multisubunit pigment–protein supercomplex found in cyanobacteria, algae, and plants, catalyzes a unique reaction in nature: the light-driven oxidation of water. Remarkable recent advances in the structural analysis of PSII now give a detailed picture of the static supercomplex on the molecular level. These data provide a solid foundation for future functional studies, in particular the mechanism of water oxidation and oxygen release.

The catalytic core of the PSII is a tetramanganese-calcium cluster (Mn_4O_5Ca), commonly referred to as the oxygen-evolving complex (OEC). The function of the OEC rests on its ability to cycle through five metastable states (S_i, $i = 0–4$), transiently storing four oxidizing equivalents, and in so doing, facilitates the four electron water splitting reaction. While the latest crystallographic model of PSII gives an atomic picture of the OEC, the exact connectivity within the inorganic core and the S-state(s) that the X-ray model represents remain uncertain.

In this Account, we describe our joint experimental and theoretical efforts to eliminate these ambiguities by combining the X-ray data with spectroscopic constraints and introducing computational modeling. We are developing quantum chemical methods to predict electron paramagnetic resonance (EPR) parameters for transition metal clusters, especially focusing on spin-projection approaches combined with density functional theory (DFT) calculations. We aim to resolve the geometric and electronic structures of all S-states, correlating their structural features with spectroscopic observations to elucidate reactivity. The sequence of manganese oxidations and concomitant charge compensation events via proton transfer allow us to rationalize the multielectron S-state cycle. EPR spectroscopy combined with theoretical calculations provides a unique window into the tetramangenese complex, in particular its protonation states and metal ligand sphere evolution, far beyond the scope of static techniques such as X-ray crystallography. This approach has led, for example, to a detailed understanding of the EPR signals in the S_2-state of the OEC in terms of two interconvertible, isoenergetic structures. These two structures differ in their valence distribution and spin multiplicity, which has important consequences for substrate binding and may explain its low barrier exchange with solvent water.

New experimental techniques and innovative sample preparations are beginning to unravel the complex sequence of substrate uptake/inclusion, which is coupled to proton release. The introduction of specific site perturbations, such as replacing Ca^{2+} with Sr^{2+}, provides discrete information about the ligand environment of the individual Mn ions. In this way, we have identified a potential open coordination site for one Mn center, which may serve as a substrate binding site in the higher S-states, such as S_3 and S_4. In addition, we can now monitor the binding of the substrate water in the lower S-states (S_1 and S_2) using new EPR-detected NMR spectroscopies. These studies provided the first evidence that one of the substrates is subsumed into the complex itself and forms an oxo-bridge between two Mn ions. This result places important new restrictions on the mechanism of O–O bond formation. These new insights from nature's water splitting catalyst provide important criteria for the rational design of bioinspired synthetic catalysts.

Published on the Web 03/18/2013 www.pubs.acs.org/accounts
10.1021/ar3003249

1. Introduction

Oxygenic photosynthesis uses a single enzyme for water splitting, Photosystem II (PSII), a multisubunit pigment-protein complex embedded in the thylakoid membrane of photosynthetic organisms such as cyanobacteria, algae, and higher plants (Figure 1a).[1] The overall reaction of PSII is that of a light-driven water:plastoquinone oxidoreductase:[2,3]

$$2H_2O + 2PQ + 4H^+_{stroma} \xrightarrow{4h\nu} O_2 + 2PQH_2 + 4H^+_{lumen} \quad (1)$$

PSII uses visible light (400−700 nm) to drive the water splitting reaction at the OEC. The chemical energy derived from this process is temporarily stored in the form of (i) reduced plastoquinone (PQ), subsequently used to generate NADPH (reduced biological hydrogen), and (ii) an electrochemical potential derived from concomitant proton transfer across the thylakoid membrane, driving ATP synthesis. NADPH and ATP are required for carbon fixation. Thus, PSII together with Photosystem I is primarily responsible for the majority of sunlight-derived biological energy storage. The reactions that occur in PSII can be divided into acceptor side (I) and donor side (II) processes:

(I) Light excitation of the reaction center (RC), a multipigment assembly of four chlorophyll-*a* and two pheophytin-*a* molecules, initiates primary charge separation, a single electron transfer process (Figure 1b), resulting in a charge-separated (radical pair) state.[4] The radical cation (primary donor), a chlorophyll pigment ($P680^{\bullet+}$), has an estimated oxidizing potential of +1.2 to +1.3 V, the highest known in biology.[5] The radical anion (primary acceptor), a pheophytin pigment (the Pheo-*a* bound to the D1 protein), and exists only transiently. The charge separated state is stabilized by subsequent electron/hole transfer steps. The acceptor passes the electron to the bound PQ molecules (Q_A and subsequently Q_B), whereas $P680^{\bullet+}$ is reduced within 100 μs by a redox active tyrosine side chain of the D1 protein, Y_Z (D1-Tyr161). In this way, the distance between the electron and the hole increases, suppressing recombination reactions. Reducing equivalents derived from this process are temporarily stored as reduced plastoquinol (Q_BH_2), a mobile electron carrier, generated after two light absorption/charge separation events.

(II) The accumulation of oxidizing equivalents on the donor side is necessary for the four-electron water-splitting oxidation reaction as the RC only generates one "electron hole" per photon absorption. Oxidizing equivalents/electron holes are stored at the site of the tetranuclear manganese complex, which is connected to the RC via the one-electron hole carrier $Y_Z^{\bullet}$. To retain charge neutrality, protons are released during accumulation of oxidizing equivalents. This has the consequence of leveling the redox transitions of the OEC such that the same oxidizing potential (about 1 V) can be used for all Mn oxidation events. The series of distinct redox intermediates that make up the water-splitting reaction cycle are described in terms of the S_i states of the Kok cycle, where i indicates the number of stored oxidizing equivalents ($i = 0-4$) in the Mn_4O_5Ca cluster[7] (Figure 1c). The S_4-state, which has not yet been spectroscopically identified, rapidly decays to S_0 upon release of molecular triplet dioxygen and the possible rebinding of one substrate water molecule. The second substrate water is only loosely bound to the Mn_4O_5Ca cluster until late in the reaction cycle, that is S_2-S_4.[13] The dark-stable or resting state of the enzyme is S_1. S_0 is of low potential such that it is oxidized via a second redox-active tyrosine residue Y_D (D2-Tyr161),[14] which does not participate further in the S-state cycle. The higher S-states, S_2 and S_3, decay back to S_1 on a time scale of seconds at room temperature.

2. Geometric Structure of the OEC

The structure of PSII from the cyanobacterium *Thermosynechococcus vulcanus* was recently determined crystallographically at a resolution of 1.9 Å by Umena et al.[6] At this resolution, the position of all four Mn ions and the Ca^{2+} of the OEC can be identified, along with the bridging oxygens connecting them. The structure of the inorganic core resembles a "distorted chair" where the base is formed by an oxo-bridged cuboidal Mn_3O_4Ca unit (Figure 2a). The fourth, "outer" Mn (Mn_{A4} in the present nomenclature, which combines the lettering used in earlier EPR and EXAFS spectroscopic work and the crystal structure numbering) is attached to this unit via a corner μ_3-oxo (O5) and a μ-oxo bridge (O4) to Mn_{B3}. The Mn_4O_5Ca core is coordinated by six carboxylate residues, three of which (Glu333, Asp342, and CP47-Glu354) form bridges between Mn ions, two (Asp170 and Ala344) bridge Ca^{2+} and Mn ions, and one (Glu189) is monocoordinated to Mn_{D1}. The cluster has only one nitrogen-donor ligand, the His332. Four water ligands are also resolved, two to Mn_{A4} (W1 and W2) and two to Ca^{2+} (W3 and W4). We note that the Ca^{2+} and at least one chloride ion close to the OEC are necessary for catalytic activity.

The S-state of the cluster as measured by X-ray crystallography is expected to represent the dark-stable S_1-state; however, this assignment is unclear as the Mn−Mn, Mn−Ca, and Mn−O/N distances in the crystallographic model

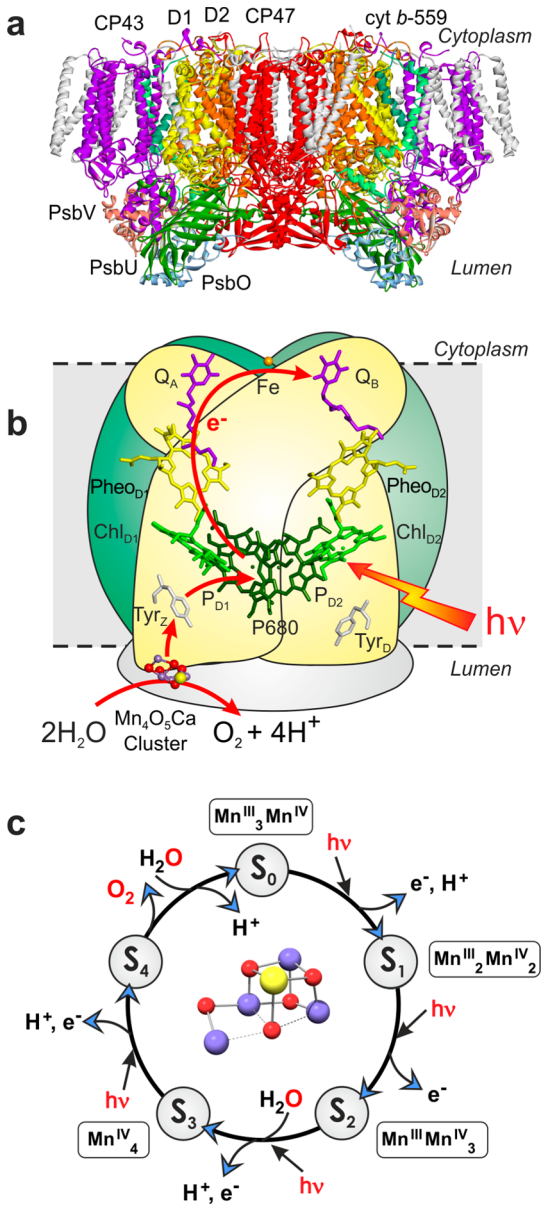

FIGURE 1. (a) X-ray crystallographic structure of the PSII dimer from *Thermosynechococcus vulcanus*[6] at 1.9 Å resolution, showing the major protein subunits in color. (b) The arrangement of cofactors in the central D1/D2 proteins involved in charge separation, electron transport, and water oxidation. (c) The S-state cycle proposed by Kok et al.,[7] showing the net oxidation state of the S_i states (high-valence model)[8−10] and the release of electrons and protons.[11,12]

are ≈0.1 Å longer compared to those determined from extended X-ray absorption fine structure (EXAFS).[17,18] Similarly, the distances between the central O5 atom and three Mn ions are not observed for any type of $Mn^{III,IV}$−O bond in any other model system, regardless of its protonation state. This suggests that the cluster underwent radiation-induced modifications, that is, photoreduction of Mn ions during data collection.[19] Thus, the X-ray model does not represent (exclusively) the S_1 but a superposition of reduced states, including nonphysiological "super-reduced" S-states (i.e., S_{-1} to S_{-3}).[20−22] Regardless, the general pattern of three short (2.7−2.8 Å) and one long (3.3 Å) Mn−Mn distances and four Mn−Ca distances (≈3.4 and ≈3.9 Å in a 2:2 or 3:1 ratio) as observed in EXAFS measurements is preserved, and thus, the crystal structure topology is similar to earlier literature models, even though the connectivity differs.

Refinements of the crystallographic model have been proposed from computational modeling.[15,16,21,23] Figure 2b shows the most recent S_2-state DFT models,[16] where O5 represents a μ-oxo bridge acting as either a bis-μ-oxo linkage between Mn_{A4} and Mn_{B3}, similar to a structure first proposed by Siegbahn,[24,25] or as a vertex of the cuboidal unit, bridging Mn_{D1}, Mn_{B3}, and the Ca^{2+} ions, reminiscent of a structure proposed by Barber and Murray.[26] DFT calculations show that these two structures are almost isoenergetic and can interconvert over a low barrier.[16] Interestingly, Kusunoki has proposed a similar type of equilibrium for the S_1-state.[27] Thus, it is likely that structural polymorphism is an inherent feature of the OEC, with implications for the phenomenology and potentially for the catalytic function described in subsequent sections.

3. The Electronic Structure of the OEC

An understanding of the electronic structure of the OEC is required to determine the mechanism of water oxidation. Electronic properties such as the spin and oxidation states of the Mn ions during the S-state cycle, and their interaction (via electronic spin exchange coupling, *J*) control the redox properties of the cluster, with consequences for substrate binding and product O_2 and H^+ release. As the water oxidation cycle involves four single oxidation events of the Mn_4O_5Ca cluster, it can be monitored by EPR. All the S-states exhibit EPR signals,[28] with S_0 and S_2 possessing half-integer spin ground states. Half-integer states can be readily measured by standard (perpendicular mode) CW-EPR and pulse EPR techniques and using these two methods, a detailed picture of the electronic structure of the OEC has been obtained for S_0 and S_2. The typical EPR signals of both S_0 and S_2-states appear at $g \approx 2$ and are called the `multiline' signals. The structure of the signals is due to the (hyperfine) interaction of the one effective (unpaired) electron spin ($S_{eff} = 1/2$) with the four ^{55}Mn nuclei. S_0 contains 26 lines, S_2 18−20 lines. As the spectral lines strongly overlap, the electronic structure cannot be uniquely determined. As a consequence, EPR-detected NMR techniques, such as ^{55}Mn-ENDOR, that probe the ^{55}Mn nuclei directly, have been

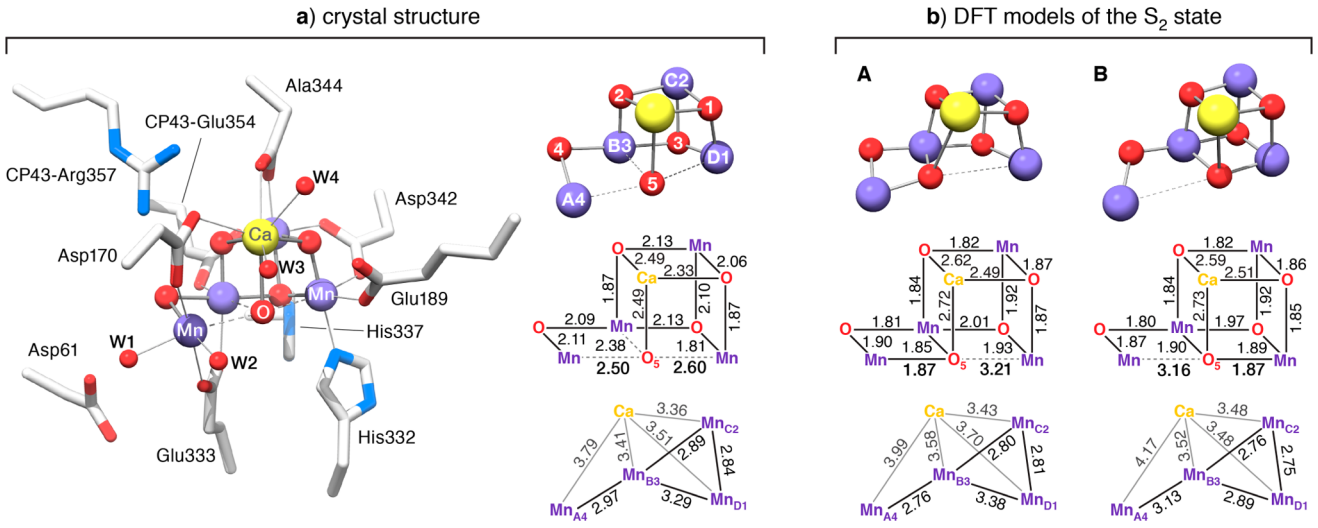

FIGURE 2. (a) X-ray crystallographic structure of the OEC in dark-adapted PSII at 1.9 Å resolution[6] and the Mn_4O_5Ca cluster from chain A of the PSII dimer. (b) Geometry-optimized DFT structures of the Mn_4O_5Ca cluster in the S_2-state: (A) model with a spin $S_{eff} = 1/2$ ground state and $g \approx 2.0$ and (B) model with an $S_{eff} = 5/2$ ground state and $g \geq 4.1$.[15,16] Both DFT structures reproduce EXAFS distance constraints and all magnetic resonance data.

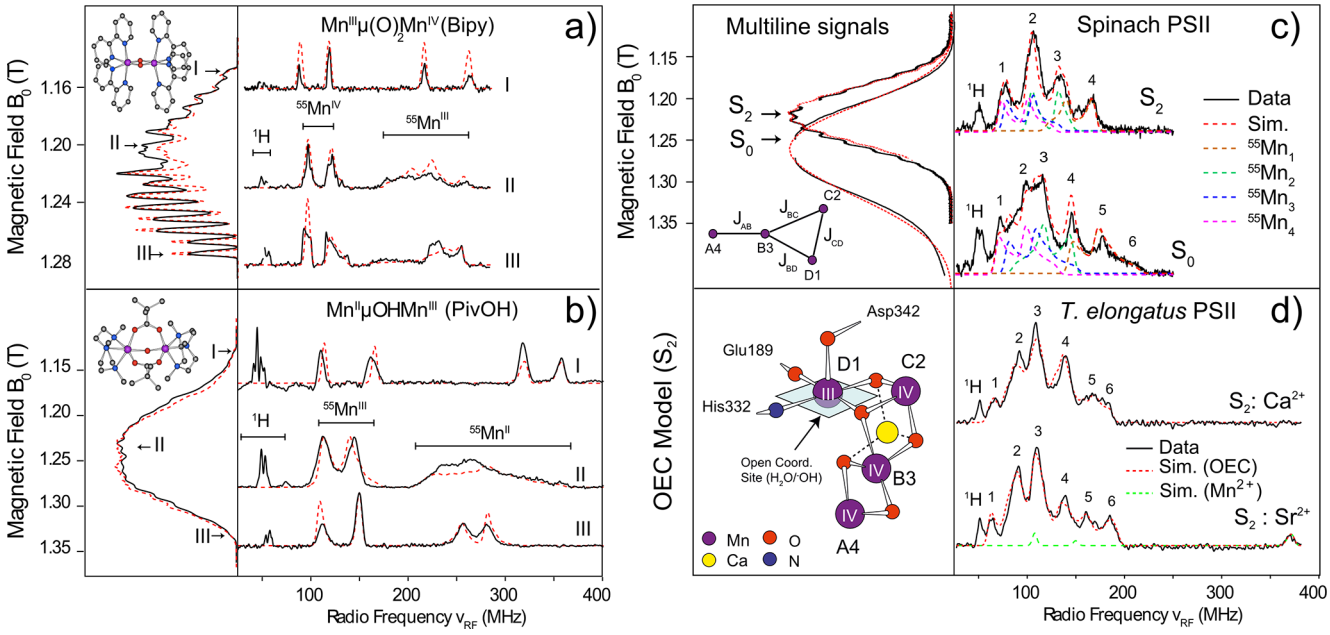

FIGURE 3. Q-band EPR (vertical) and ^{55}Mn-ENDOR (horizontal) spectra of the OEC and related model systems and their atomic structures. (a) Mn^{III}-(μ-O)$_2$-Mn^{IV} (Bipy). (b) Mn^{II}-(μ-OH)-Mn^{III} (PivOH).[32] (c) The S_2 and S_0 OEC states in spinach PSII (4% methanol),[8] (d) the S_2-state from native *T. elongatus* (Ca^{2+}) and from *T. elongatus* phototrophically grown in Sr^{2+} media; the corresponding EPR spectra are essentially the same as the S_2 multiline in panel (c).[33] Black lines represent the experimental data and red dashed lines represent simulations based on the spin-Hamiltonian formalism. The arrows/roman numerals in (a) and (b) show the position where the ENDOR spectrum was recorded within the EPR signal profile; see ref 32 for details. In the panel next to (d), the EPR/^{55}Mn-ENDOR-derived S_2 structural model for the S_2-state is shown with the assigned distribution of Mn oxidation states. Panels are adapted from ref.[8,32−33]

developed to more accurately characterize the electronic structure.[29−31]

^{55}Mn-ENDOR data for the OEC are shown in Figure 3c and d. The key observation is that the entire ^{55}Mn-ENDOR envelope appears over a very small frequency range, smaller than that of model complexes such as exchange-coupled Mn dimers (Figure 3a and b). This requires that all four Mn ions of the OEC carry significant electron spin density. That is to say, all four Mn contribute approximately equally to the electronic ground state of the complex, a circumstance not seen in models where one Mn center typically carries a majority of electron spin. In addition, the narrow spectral breadth of

the ^{55}Mn-ENDOR envelope in both the S_2 and S_0 states requires that the OEC does not contain a Mn^{II} ion in any S-state during its reaction cycle, and thus restricts the net oxidation states of the S_0- and S_2-states to be Mn_4(III,III,III, IV) and Mn_4(III,IV,IV,IV), respectively, to yield the experimentally observed spin multiplicity.[8] These oxidation state assignments are consistent with results inferred from X-ray spectroscopy;[9,10] although see ref 34 for an alternative assignment.

4. Mapping the Electronic Structure to the Geometric Structure

Recently broken-symmetry DFT methods have been developed to calculate magnetic resonance parameters for oligonuclear transition metal complexes and has fundamentally changed our understanding of the electronic structure of the OEC.[35−37] It has allowed unified models of the OEC to be developed from crystallographic information, which simultaneously reproduce structural constraints from X-ray spectroscopy and magnetic resonance data.[15,16] We have used DFT to assess OEC structural candidates that differ in conformation, protonation patterns, and oxidation states. Our work has primarily focused on the S_2-state and has converged around an "open cubane" topology for the OEC,[25] with the Mn^{III} ion as part of the trimer unit (Mn_{D1}).[15] This is supported by site perturbations of the cluster such as Ca^{2+}/Sr^{2+} ion exchange, the large ^{14}N coupling measured for the histidine coordinating Mn_{D1} (D1-His332),[38,39] and orientation-dependent EPR/^{55}Mn-ENDOR data on PSII single crystals.[40]

By this combination of quantum chemistry and spectroscopy, we recently addressed a long-standing question concerning the presence of two interconvertible EPR signals in the S_2-state of the OEC.[16] These two signals, the multiline and $g \geq 4.1$, represent two energetically similar but electronically/structurally distinct, conformations of the Mn tetramer, which can be interconverted by the absorption of infrared light at low temperature.[41] As described above, two quasi-isoenergetic and interconvertible minima were located for the S_2-state (Figure 2b). Structurally, they differ in the position of O5 and its bonding with the terminal Mn ions, Mn_{D1} and Mn_{A4}. Most importantly, they differ electronically in the distribution of oxidation states (the location of the only Mn^{III} ion of the S_2-state) and the magnetic coupling between the Mn ions, leading to distinct ground spin states and spectroscopic signatures for the two conformations (Figure 4 and Table 1). The "open" form A in Figure 2b has a spin $S_G = 1/2$ ground state and gives rise to the multiline EPR signal centered at $g \approx 2$. On the other hand, the "closed" cubane structure (model B of Figure 2b) displays a ground spin $S_G = 5/2$ and gives rise to the high-g signals ($g \geq 4.1$) associated with the OEC.[16]

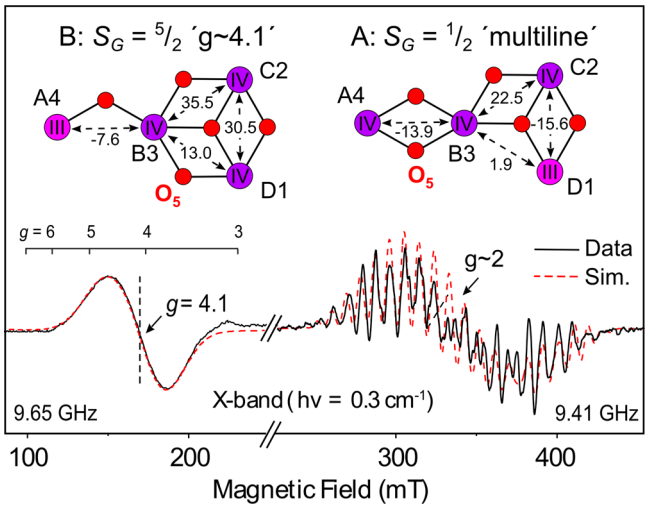

FIGURE 4. Manganese oxidation state distributions and exchange coupling Mn−Mn interactions (cm^{-1}) in the S_2-state models A and B (Figure 2b), and their corresponding EPR signals adapted from refs 28 and 33. The Ca^{2+} is omitted for clarity.

TABLE 1. EPR Simulation Parameters for S_2-State DFT Models A and B (Figure 2b) Compared to Experimental Data

	DFT models[15,16]		experimental results	
$\lvert A_{iso}\rvert$ /MHz	model A	model B	multiline[33,38]	$g \geq 4.1$[28]
Mn_{D1}	197	85	251	
Mn_{C2}	199	85	208	87 ($A_{avg/4Mn}$)
Mn_{B3}	182	73	191	
Mn_{A4}	306	103	312	
^{14}N (His332)	5.2	–	6.95	–
$\lvert D\rvert$/cm^{-1} (E/D)	–	0.2−1.2 (0.25)	–	0.45 (0.25)
ΔE_{ES-GS} /cm^{-1}	23.2	16.4	23.5	–

In addition to rationalizing the two basic EPR signals of the S_2-state as arising from two electronically distinct structural isomers, these DFT models also appear to explain the complicated phenomenology of the OEC seen under various preparative conditions and reveal its possible inherent dynamic nature. It is seen that modulation of the electronic connectivity between the outer Mn_{A4} and the three remaining Mn ions provides a simple rationale for many experimental observations including (i) spectral variation among different species such as cyanobacteria and higher plants;[42] (ii) the influence of small molecules, such as methanol, on the exact line shape;[42] and (iii) modifications due to substitution of Ca^{2+} for Sr^{2+}, or Ca^{2+} removal.[33,43] The monomer−trimer junction is structurally the most solvent-accessible region of the OEC, allowing small molecules to interact with the Mn_{A4} ion, potentially via displacement of its water ligands.

Similarly, as the Ca^{2+} forms part of the linkage between the outer Mn_{A4} and the trimer, its replacement by Sr^{2+} or its removal is also expected to perturb the Mn monomer-trimer interaction.

It is noted that an alternative S_2 state model has been proposed by Pace and co-workers[34] assuming a lower net oxidation state i.e. $(Mn^{III})_3Mn^{IV}$. Their DFT structures do not reproduce the EXAFS Mn−Mn distance constraints or magnetic resonance data detailed in sections 3 and 4.

5. Substrate Binding to the OEC

The OEC represents a genuine molecular catalyst with only two sites for substrate binding, resulting in single product formation, namely O_2, as opposed to other reactive radical oxygen species ($H_2O_2/HO_2^-/O_2^{\bullet-}$). The sites of substrate binding have been extensively studied using time-resolved membrane-inlet mass spectrometry (MIMS) which monitors the rate at which labelled ($H_2{}^{18}O$) water is exchanged into substrate sites of the Mn_4O_5Ca cluster.[13] These experiments identify Ca^{2+} as a site of substrate water binding as the substrate's exchange with bulk water is influenced by biochemical Ca^{2+}/Sr^{2+} replacement. In addition, these measurements demonstrate that the two substrate water molecules bind at chemically different sites. The early binding substrate water (W_s) exchanges slowly with bulk water in all S_i states suggesting that it binds at the start of the S-state cycle (S_0), while the late binding substrate (W_f) exchanges rapidly in all S-states, with the rate of exchange only resolved in the S_2 and S_3 states. Results from FTIR support this model, suggesting that W_f binds during the $S_2 \rightarrow S_3$ transition.[44]

EPR spectroscopy allows the location and protonation state ($H_2O/OH^-/O^{2-}$) of exchangeable water sites of the Mn_4O_5Ca to be identified. This can be achieved via the detection of the coupling of magnetic nuclei [$^1H/^2H$ (I = 1/2, 1) or ^{17}O ($I = 5/2$)] to the $S_{eff} = 1/2$ states (S_0, S_2) of the Mn_4O_5Ca cluster. Recently, we have addressed this topic using high-field ^{17}O-EDNMR (Electron−Electron-Double Resonance-Detected NMR)[45] observing exchangeable ^{17}O "water" signals (Figure 5a). Importantly, all ^{17}O signals are observed after only short incubations (<15 s) in the labelled solvent water ($H_2{}^{17}O$), the same timescale as substrate exchange as inferred from the MIMS experiment. Three classes of nuclei were assigned by comparison with ^{17}O-labeled model complexes: (i) a μ-oxo bridge; (ii) terminal $Mn_{A4}-OH/OH_2$; and (iii) Ca^{2+}-bound 2nd shell OH^-/H_2O ligands. The exchangeable μ-oxo bridge was assigned to either O4 or O5 (Figure 5b). A similar μ-oxo bridge signal was observed in Q-band ^{17}O-ENDOR experiments.[46]

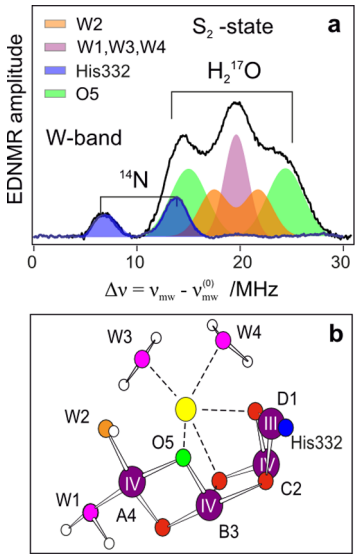

FIGURE 5. (a) ^{17}O-ELDOR-detected NMR spectra (94 GHz) of the OEC exchanged in $H_2{}^{17}O$ and poised in the S_2-state.[45] (b) Structure of the Mn_4O_5Ca cluster with μ-oxo bridges and bound water molecules W1 to W4. Mn, purple; Ca, yellow; N, blue; H, white; O (nonexchangeable), red; O (exchangeable), pink/orange/green) Panels are adapted from ref.[45]

Results from FTIR spectroscopy also suggest that the OEC contains an exchangeable μ_2-oxo or μ_3-oxo bridge. In the higher plant study of Chu et al.,[47] a Mn−O mode was identified in the S_2-S_1 difference spectrum assigned by comparison to model Mn (di-μ-oxo) and related Mn/Fe complexes. Interestingly, this same mode was sensitive to Sr^{2+} substitution, suggesting that it also represents a bridge to Ca^{2+}/Sr^{2+}, i.e. O5.

The result that a Mn μ-oxo bridge of the Mn_4O_5Ca complex exchanges on a seconds timescale, similar to that of the substrate, is unexpected. Similar μ-oxo bridge exchange rates have not been observed in in synthetic[48] and biological model systems.[46] Presumably this is because these models lack structural features of the OEC, including nearby acid/base derivatives which could couple oxygen inclusion with proton release/uptake. Similarly, the OEC appears to contain several pathways for internal oxygen-exchange between terminal water ligands to Ca^{2+} (or Mn), which may allow a calcium-ligated bridge such as O5 to exchange rapidly.[11,48] We note that the theoretical rationalization of the two electronic and structural forms of the S_2-state that give rise to the multiline and $g \geq 4.1$ EPR signals reflects the facile movement of the O5 bridge.[16] This unique structural flexibility of the O5 provides additional support for its assignment to the solvent exchangeable μ-oxo bridge and as one of the substrate water sites.

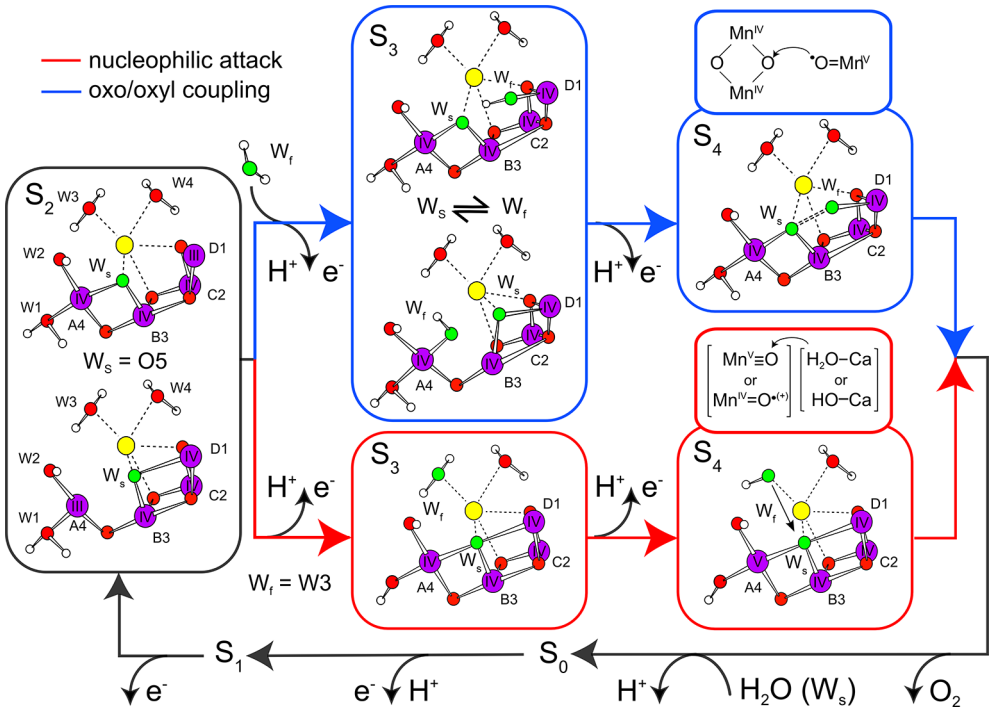

FIGURE 6. Possible catalytic pathways of O–O bond formation: (I) nucleophilic attack (red boxes) and (II) oxo/oxyl radical coupling (blue boxes). The $Mn_{A4}(V)\equiv O$ may equally be considered a $Mn(IV)=O^{\bullet(+)}$ species. The flexibility of the OEC in the S_2-state (and presumably other *S*-states) is potentially critical for fast water exchange and possibly for the second substrate water binding, which a growing body of evidence associates with the formation of the S_3-state.

6. Consequences for the Mechanism of O–O Bond Formation

As described above, a series of recent studies are converging with regard to the role of O5 as the W_S substrate site, limiting the number of reaction pathways for O–O bond formation. In particular, this assignment readily explains both the oxidation state dependence[49] and influence of Ca^{2+}/Sr^{2+} substitution[13,50] on exchange kinetics of the slowly exchanging substrate water (W_s). O–O bond formation involving O5 can proceed via either[51] (I) a nucleophilic attack of the O5 (μ-oxo bridge) by W3 (Ca^{2+}-bound hydroxide ion/water) or (II) an oxo/oxyl radical coupling between O5 and an as yet unidentified water (possibly coming from the Ca^{2+} or the Mn_{A4} ion) that is located proximal to O5 in S_3/S_4, as proposed by Siegbahn.[24]

Evidence exists in the current literature that supports a nucleophilic attack mechanism in Mn model systems that perform O–O bond formation, but these models exhibit turnover frequencies orders of magnitude slower than the OEC.[52,53] In contrast, the radical coupling mechanism has no precedence in Mn model chemistry but has been experimentally demonstrated via isotopic labeling as an energetically favorable pathway for efficient O–O bond formation in second-row transition metal catalysts; see, for example, the ruthenium (Ru-Hbpp) dimer complex.[54] And it is this mechanistic route that has *in silico* been shown by Siegbahn as the most efficient O–O bond formation pathway.[24] In his concerted tetramer mechanism, the unique geometry of the Mn_4O_5Ca cluster is used to bind and position the two substrates and excludes the simultaneous binding of both substrates in the resting states (S_0, S_1) of the catalyst, a potential explanation for the high selectivity of the OEC toward O_2 formation, disfavoring "catalase-like" two-electron chemistry.

The two mechanistic pathways differ upon formation of S_3. In a nucleophilic attack, the complex must contract, with O5 now a genuine ligand to both Mn_{D1} and Mn_{A4} (Figure 6), within the assumption that the $S_2 \rightarrow S_3$ transition represents a Mn-centered oxidation, that is, the net oxidation states in S_3 are Mn$_4$(IV,IV,IV,IV). In contrast, in the oxo/oxyl radical coupling mechanism, an additional water molecule must bind to the cluster requiring the complex to expand upon S_3 formation. In the Siegbahn mechanism, this additional substrate (the fast-exchanging W_f) binds at the open coordination site of Mn_{D1} as a water/hydroxide ion in the S_3-state, forming an oxyl radical in S_4 (Figure 6).[24]

The requirement that both substrate sites are exchangeable with bulk water in all *S*-states and the rates of exchange are similar in both S_2 and S_3, provides a means to discriminate between these two basic reaction pathways, favoring oxo/oxyl coupling. For the nucleophilic attack mechanism, the exchangeability of O5 would be expected to decrease upon this step as it is further subsumed into an all-Mn^{IV} complex. The same is

unlikely to be the case for the oxo/oxyl coupling mechanism as the binding of an additional water/hydroxide ion in S_3 provides yet another molecular pathway for O5 exchange. Indeed, the dynamic nature of the OEC in the S_2 and possibly the S_3-state could again play a role here, facilitating the binding of the second substrate via the solvent-accessible outer Mn_{A4} ion, which upon proton rearrangement returns to the putative S_3-state proposed by Siegbahn. In this instance, the terminal water ligands of the Mn_{A4} (i.e., W1/W2) and W_f may not be distinguishable, owing to rapid interchange about the $Mn_{A4}-O4$ bond.

The essential challenge for experimentalists is to demonstrate if radical oxyl chemistry is possible for a first row transition metal such as manganese; that is to say, whether a Mn^{IV}-oxyl state is energetically accessible. No evidence exists within the current literature of model complexes of this electronic configuration, but an analogous complex, a putative Mn^{III}-oxyl, has been reported.[55] Theoretical studies of this complex, a mononuclear Mn center supported by a salen-like ligand scaffold, suggest the Mn^{III}-oxyl and Mn^{IV}-oxo electronic configurations are essentially isoenergetic, unlike that of other transition metals such as iron. This electronic flexibility of manganese may account for its adoption by nature to perform biological water splitting, simultaneously allowing the deprotonation and translocation of substrate water (Figure 6, blue boxes) and ligand (oxygen)-centered oxidation during the $S_3 \rightarrow S_4$ transition.

Dr. William Ames and Dr. Johannes Messinger are acknowledged for their important contribution to the sections describing second substrate binding and substrate water exchange. Financial support was provided by the Max Planck Society, and the EU SOLAR-H2 program (FP7 contract 212508).

BIOGRAPHICAL INFORMATION

Nicholas Cox (07/16/1981, Canberra, Australia) received his Ph.D. (2008) in Chemistry from the Australian National University, subsequently undertaking a postdoctoral fellowship at the Max-Planck Institute (MPI) for Bioinorganic Chemistry. He is currently a group leader at the MPI for Chemical Energy Conversion. His research has focused on the study of biological enzymes primarily using magnetic resonance techniques.

Dimitrios A. Pantazis (06/21/1976, Ioannina, Greece) received a Ph.D. (2006) in Chemistry from the University of York, United Kingdom and worked as a postdoctoral fellow at the Universities of Glasgow and Bonn (2006–2011). Since 2011, he is a group leader at the MPI for Chemical Energy Conversion. His research focuses on the development and application of quantum chemical approaches for the study of the magnetism, spectroscopy, and reactivity of inorganic and bioinorganic systems.

Frank Neese (12/13/1967, Wiesbaden, Germany) received his Doctorate (Dr. rer. nat., 1997) and Habilitation at the University of Konstanz, Germany and undertook postdoctoral work at Stanford University with Prof. E. I. Solomon (1997–1999), before joining the MPI for Bioinorganic Chemistry in 2001 as a group leader, until accepting the position of full professor and Chair of Theoretical Chemistry at the University of Bonn (2006). In 2011, he became director of the MPI for Chemical Energy Conversion (Department of Molecular Theory and Spectroscopy). His work focuses on the theory of magnetic spectroscopies and their experimental and theoretical application. He is the lead author of the ORCA program.

Wolfgang Lubitz (07/23/1949, Berlin, Germany) received his Doctorate (Dr. rer. nat., 1977) and Habilitation at the Free University of Berlin and undertook a postdoctoral fellowship at the UC San Diego (1983–1984) with Prof. G. Feher. After associate professorships at the Free University (1986–1989) and the University of Stuttgart (1989–1991), he became a full professor at the Max Volmer Institute (TU Berlin). In 2000, he became director at the MPI for Bioinorganic Chemistry, now Chemical Energy Conversion. His research is primarily focused on the development of magnetic resonance techniques, especially EPR for the study of biological systems, with regard to electron transfer and catalysis.

FOOTNOTES

*To whom correspondence should be addressed. (N.C.) Telephone: +49-208-306-3552. E-mail: Nicholas.Cox@cec.mpg.de. (W.L.) Telephone: +49-208-306-3614. E-mail: Wolfgang.Lubitz@cec.mpg.de.

The authors declare no competing financial interest.

REFERENCES

1 Kargul, J.; Barber, J. In *Molecular Solar Fuels*; Wydrzynski, T., Hillier, W., Eds.; The Royal Society of Chemistry: Cambridge, U.K., 2012; pp 107–142.

2 Hillier, W.; Messinger, J. Mechanism of photosynthetic oxygen production. In *Photosystem II: The Light-Driven Water: Plastoquinone Oxidoreductase*, Wydrzynski, T. J. and Satoh, K., Eds., Volume 22, Advances in Photosynthesis and Respiration, Springer, Dordrecht, The Netherlands.

3 McEvoy, J. P.; Brudvig, G. W. Water-splitting chemistry of photosystem II. *Chem. Rev.* **2006**, *106*, 4455–4483.

4 Cardona, T.; Sedoud, A.; Cox, N.; Rutherford, A. W. Charge separation in Photosystem II: a comparative and evolutionary overview. *Biochim. Biophys. Acta* **2012**, *1817*, 26–43.

5 Rappaport, F.; Guergova-Kuras, M.; Nixon, P. J.; Diner, B. A.; Lavergne, J. Kinetics and Pathways of Charge Recombination in Photosystem II. *Biochemistry* **2002**, *41*, 8518–8527.

6 Umena, Y.; Kawakami, K.; Shen, J.-R.; Kamiya, N. Crystal structure of oxygen-evolving photosystem II at a resolution of 1.9 Å. *Nature* **2011**, *473*, 55–60.

7 Kok, B.; Forbush, B.; McGloin, M. Cooperation of charges in photosynthetic O_2 evolution-1. A linear four step mechanism. *Photochem. Photobiol.* **1970**, *11*, 457–467.

8 Kulik, L. V.; Epel, B.; Lubitz, W.; Messinger, J. Electronic structure of the Mn_4O_xCa cluster in the S_0 and S_2 states of the oxygen-evolving complex of photosystem II based on pulse ^{55}Mn ENDOR and EPR Spectroscopy. *J. Am. Chem. Soc.* **2007**, *129*, 13421–13435.

9 Bergmann, U.; Grush, M. M.; Horne, C. R.; DeMarois, P.; Penner-Hahn, J. E.; Yocum, C. F.; Wright, D. W.; Dube; Armstrong, W. H.; Christou, G.; Eppley, H. J.; Cramer, S. P. Characterization of the Mn Oxidation States in Photosystem II by K_β X-ray Fluorescence Spectroscopy. *J. Phys. Chem. B* **1998**, *102*, 8350–8352.

10 Roelofs, T. A.; Liang, W.; Latimer, M. J.; Cinco, R. M.; Rompel, A.; Andrews, J. C.; Sauer, K.; Yachandra, V. K.; Klein, M. P. Oxidation states of the manganese cluster during the flash-induced S-state cycle of the photosynthetic oxygen-evolving complex. *Proc. Natl. Acad. Sci. U.S.A.* **1996**, *93*, 3335–3340.

11 Messinger, J.; Renger, G. In *Primary Processes of Photosynthesis - Part 2: Basic Principles and Apparatus*; Renger, G., Ed.; Royal Society of Chemistry: Cambridge, 2008; pp 291–349.

12 Dau, H.; Haumann, M. The manganese complex of photosystem II in its reaction cycle - basic framework and possible realization at the atomic level. *Coord. Chem. Rev.* **2008**, *252*, 273–295.

13 Hillier, W.; Wydrzynski, T. ^{18}O-Water exchange in photosystem II: Substrate binding and intermediates of the water splitting cycle. *Coord. Chem. Rev.* **2008**, *252*, 306–317.

14 Styring, S.; Rutherford, A. W. In the oxygen-evolving complex of photosystem II the S_0 state is oxidized to the S_1 state by D^+ (signal II_{slow}). *Biochemistry* **1987**, *26*, 2401–2405.

15 Ames, W.; Pantazis, D. A.; Krewald, V.; Cox, N.; Lubitz, W.; Neese, F. Theoretical evaluation of structural models of the S_2 state in the oxygen evolving complex of photosystem II: protonation states and magnetic interactions. *J. Am. Chem. Soc.* **2011**, *133*, 19743–19757.

16 Pantazis, D. A.; Ames, W.; Cox, N.; Lubitz, W.; Neese, F. Two Interconvertible Structures that Explain the Spectroscopic Properties of the Oxygen-Evolving Complex of Photosystem II in the S_2 State. *Angew. Chem., Int. Ed.* **2012**, *51*, 9935–9940.

17 Yano, J.; Kern, J.; Sauer, K.; Latimer, M. J.; Pushkar, Y.; Biesiadka, J.; Loll, B.; Saenger, W.; Messinger, J.; Zouni, A.; Yachandra, V. K. Where Water Is Oxidized to Dioxygen: Structure of the Photosynthetic Mn_4Ca Cluster. *Science* **2006**, *314*, 821–825.

18 Pushkar, Y. L.; Yano, J.; Sauer, K.; Boussac, A.; Yachandra, V. K. Structural changes in the Mn_4Ca cluster and the mechanism of photosynthetic water splitting. *Proc. Natl. Acad. Sci. U.S.A.* **2008**, *105*, 1879–1884.

19 Yano, J.; Kern, J.; Irrgang, K.-D.; Latimer, M. J.; Bergmann, U.; Glatzel, P.; Pushkar, Y.; Biesiadka, J.; Loll, B.; Sauer, K.; Messinger, J.; Zouni, A.; Yachandra, V. K. X-ray damage to the Mn_4Ca complex in single crystals of photosystem II: A case study for metalloprotein crystallography. *Proc. Natl. Acad. Sci. U.S.A.* **2005**, *102*, 12047–12052.

20 Grundmeier, A.; Dau, H. Structural models of the manganese complex of photosystem II and mechanistic implications. *Biochim. Biophys. Acta Bioenerg.* **2012**, *1817*, 88–105.

21 Luber, S.; Rivalta, I.; Umena, Y.; Kawakami, K.; Shen, J. R.; Kamiya, N.; Brudvig, G. W.; Batista, V. S. S_1-State Model of the O_2-Evolving Complex of Photosystem II. *Biochemistry* **2011**, *50*, 6308–6311.

22 Galstyan, A.; Robertazzi, A.; Knapp, E. W. Oxygen−evolving Mn cluster in photosystem II: the protonation pattern and oxidation state in the high−resolution crystal structure. *J. Am. Chem. Soc.* **2012**, *134*, 7442–7449.

23 Isobe, H.; Shoji, M.; Yamanaka, S.; Umena, Y.; Kawakami, K.; Kamiya, N.; Shen, J. R.; Yamaguchi, K. Theoretical illumination of water-inserted structures of the $CaMn_4O_5$ cluster in the S_2 and S_3 states of oxygen-evolving complex of photosystem II: full geometry optimizations by B3LYP hybrid density functional. *Dalton Trans.* **2012**, *41*, 13727–13740.

24 Siegbahn, P. E. M. Structures and Energetics for O_2 Formation in Photosystem II. *Acc. Chem. Res.* **2009**, *42*, 1871–1880.

25 Siegbahn, P. E. M. A structure consistent mechanism for dioxygen formation in photosystem II. *Chem.—Eur. J.* **2008**, *14*, 8290–8302.

26 Barber, J.; Murray, J. W. The structure of the Mn_4Ca^{2+} cluster of photosystem II and its protein environment as revealed by X-ray crystallography. *Phil. Trans. R. Soc. B* **2008**, *363*, 1129–1137.

27 Kusunoki, M. S_1-state Mn_4Ca complex of Photosystem II exists in equilibrium between the two most-stable isomeric substates: XRD and EXAFS evidence. *J. Photochem. Photobiol., B* **2011**, *104*, 100–110.

28 Haddy, A. EPR spectroscopy of the manganese cluster of photosystem II. *Photosynth. Res.* **2007**, *92*, 357–368.

29 Randall, D. W.; Sturgeon, B. E.; Ball, J. A.; Lorigan, G. A.; Chan, M. K.; Klein, M. P.; Armstrong, W. H.; Britt, R. D. ^{55}Mn ESE-ENDOR of a Mixed Valence Mn(III)Mn(IV) Complex: Comparison with the Mn Cluster of the Photosynthetic Oxygen-Evolving Complex. *J. Am. Chem. Soc.* **1995**, *117*, 11780–11789.

30 Peloquin, J. M.; Campbell, K. A.; Randall, D. W.; Evanchik, M. A.; Pecoraro, V. L.; Armstrong, W. H.; Britt, R. D. ^{55}Mn ENDOR of the S_2-state multiline EPR signal of photosystem II: Implications on the structure of the tetranuclear Mn cluster. *J. Am. Chem. Soc.* **2000**, *122*, 10926–10942.

31 Kulik, L. V.; Epel, B.; Lubitz, W.; Messinger, J. ^{55}Mn pulse ENDOR at 34 GHz of the S_0 and S_2 states of the oxygen-evolving complex in photosystem II. *J. Am. Chem. Soc.* **2005**, *127*, 2392–2393.

32 Cox, N.; Ames, W.; Epel, B.; Kulik, L. V.; Rapatskiy, L.; Neese, F.; Messinger, J.; Wieghardt, K.; Lubitz, W. Electronic Structure of a Weakly Antiferromagnetically Coupled $Mn^{II}Mn^{III}$ Model Relevant to Manganese Proteins: A Combined EPR, ^{55}Mn-ENDOR, and DFT Study. *Inorg. Chem.* **2011**, *50*, 8238–8251.

33 Cox, N.; Rapatskiy, L.; Su, J.-H.; Pantazis, D. A.; Sugiura, M.; Kulik, L.; Dorlet, P.; Rutherford, A. W.; Neese, F.; Boussac, A.; Lubitz, W.; Messinger, J. Effect of Ca^{2+}/Sr^{2+} Substitution on the Electronic Structure of the Oxygen-Evolving Complex of Photosystem II: A Combined Multifrequency EPR, ^{55}Mn-ENDOR and DFT study of the S_2 state. *J. Am. Chem. Soc.* **2011**, *133*, 3635–3648.

34 Jaszewski, A. R.; Petrie, S.; Pace, R. J.; Stranger, R. Toward the Assignment of the Manganese Oxidation Pattern in the Water-Oxidizing Complex of Photosystem II: A Time-Dependent DFT Study of XANES Energies. *Chem.—Eur. J.* **2011**, *17*, 5699–5713.

35 Pantazis, D. A.; Orio, M.; Petrenko, T.; Zein, S.; Bill, E.; Lubitz, W.; Messinger, J.; Neese, F. A new quantum chemical approach to the magnetic properties of oligonuclear transition-metal complexes: Application to a model for the tetranuclear manganese cluster of Photosystem II. *Chem.—Eur. J.* **2009**, *15*, 5108–5123.

36 Orio, M.; Pantazis, D. A.; Neese, F. Density Functional Theory. *Photosynth. Res.* **2009**, *102*, 443–453.

37 Pantazis, D. A.; Orio, M.; Petrenko, T.; Zein, S.; Lubitz, W.; Messinger, J.; Neese, F. Structure of the oxygen-evolving complex of photosystem II: information on the S_2 state through quantum chemical calculation of its magnetic properties. *Phys. Chem. Chem. Phys.* **2009**, *11*, 6788–6798.

38 Stich, T. A.; Yeagle, G. J.; Service, R. J.; Debus, R. J.; Britt, R. D. Ligation of D1-His332 and D1-Asp170 to the Manganese Cluster of Photosystem II from Synechocystis Assessed by Multifrequency Pulse EPR Spectroscopy. *Biochemistry* **2011**, *50*, 7390–7404.

39 Schinzel, S.; Schraut, J.; Arbuznikov, A.; Siegbahn, P.; Kaupp, M. Density Functional Calculations of ^{55}Mn, ^{14}N and ^{13}C Electron Paramagnetic Resonance Parameters Support an Energetically Feasible Model System for the S_2 State of the Oxygen-Evolving Complex of Photosystem II. *Chem.—Eur. J.* **2010**, *16*, 10424–10438.

40 Teutloff, C.; Pudollek, S.; Kessen, S.; Broser, M.; Zouni, A.; Bittl, R. Electronic structure of the tyrosine D radical and the water-splitting complex from pulsed ENDOR spectroscopy on photosystem II single crystals. *Phys. Chem. Chem. Phys.* **2009**, *11*, 6715–6726.

41 Boussac, A.; Girerd, J.-J.; Rutherford, A. W. Conversion of the Spin State of the Manganese Complex in Photosystem II Induced by Near-Infrared Light. *Biochemistry* **1996**, *35*, 6984–6989.

42 Su, J. H.; Cox, N.; Ames, W.; Pantazis, D. A.; Rapatskiy, L.; Lohmiller, T.; Kulik, L.; Dorlet, P.; Rutherford, A. W.; Neese, F.; Boussac, A.; Lubitz, W.; Messinger, J. The electronic structures of the S_2 states of the oxygen-evolving complexes of photosystem II in plants and cyanobacteria in the presence and absence of methanol. *Biochim. Biophys. Acta* **2011**, *1807*, 829–840.

43 Lohmiller, T.; Cox, N.; Su, J. H.; Messinger, J.; Lubitz, W. The Basic Properties of the Electronic Structure of the Oxygen-evolving Complex of Photosystem II Are Not Perturbed by Ca^{2+} Removal. *J. Biol. Chem.* **2012**, *287*, 24721–33.

44 Noguchi, T. FTIR detection of water reactions in the oxygen-evolving centre of photosystem II. *Phil. Trans. R. Soc. B* **2008**, *363*, 1189–1195.

45 Rapatskiy, L.; Cox, N.; Savitsky, A.; Ames, W. M.; Sander, J.; Nowaczyk, M. M.; Rögner, M.; Boussac, A.; Neese, F.; Messinger, J.; Lubitz, W. Detection of the Water Binding Sites of the Oxygen-evolving Complex of Photosystem II Using W-band ^{17}O ELDOR-detected NMR Spectroscopy. *J. Am. Chem. Soc.* **2012**, *134*, 16619–16634.

46 McConnell, I. L.; Grigoryants, V. M.; Scholes, C. P.; Myers, W. K.; Chen, P. P. Y.; Whittaker, J. W.; Brudvig, G. W. EPR-ENDOR Characterization of (^{17}O, ^{1}H, ^{2}H) Water in Manganese Catalase and its Relevance to the Oxygen-Evolving Complex of Photosystem II. *J. Am. Chem. Soc.* **2012**, *134*, 1504–1512.

47 Chu, H.-A.; Sackett, H.; Babcock, G. T. Identification of a Mn-O-Mn Cluster Vibrational Mode of the Oxygen-Evolving Complex in Photosystem II by Low-Frequency FTIR Spectroscopy. *Biochemistry* **2000**, *39*, 14371–14376.

48 Tagore, R.; Crabtree, R. H.; Brudvig, G. W. Distinct Mechanisms of Bridging-Oxo Exchange in Di-μ-O Dimanganese Complexes with and without Water-Binding Sites: Implications for Water Binding in the O_2-Evolving Complex of Photosystem II. *Inorg. Chem* **2007**, *46*, 2193–2203.

49 Hillier, W.; Wydrzynski, T. The Affinities for the Two Substrate Water Binding Sites in the O_2-Evolving Complex of Photosystem II Vary Independently during S-State Turnover. *Biochemistry* **2000**, *39*, 4399–4405.

50 Hendry, G.; Wydrzynski, T. ^{18}O isotope exchange measurements reveal that calcium is involved in the binding of one substrate-water molecule to the oxygen-evolving complex in photosystem II. *Biochemistry* **2003**, *42*, 6209–6217.

51 Yamanaka, S.; Isobe, H.; Kanda, K.; Saito, T.; Umena, Y.; Kawakami, K.; Shen, J. R.; Kamiya, N.; Okumura, M.; Nakamura, H.; Yamaguchi, K. Possible mechanisms for the O−O bond formation in oxygen evolution reaction at the $CaMn_4O_5(H_2O)_4$ cluster of PSII refined to 1.9 Å X-ray resolution. *Chem. Phys. Lett.* **2011**, *511*, 138–145.

52 Gao, Y.; Åkermark, T.; Liu, J.; Sun, L.; Åkermark, B. Nucleophilic Attack of Hydroxide on a Mn^V Oxo Complex: A Model of the O-O Bond Formation in the Oxygen Evolving Complex of Photosystem II. *J. Am. Chem. Soc.* **2009**, *131*, 8726–8727.

53 Privalov, T.; Sun, L.; Åkermark, B.; Liu, J.; Gao, Y.; Wang, M. A Computational Study of O-O Bond Formation Catalyzed by Mono- and Bis-Mn^{IV} Corrole Complexes. *Inorg. Chem.* **2007**, *46*, 7075–7086.

54 Romain, S.; Bozoglian, F.; Sala, X.; Llobet, A. Oxygen-Oxygen Bond Formation by the Ru-Hbpp Water Oxidation Catalyst Occurs Solely via an Intramolecular Reaction Pathway. *J. Am. Chem. Soc.* **2009**, *131*, 2768–2769.

55 Lassalle-Kaiser, B.; Hureau, C.; Pantazis, D. A.; Pushkar, Y.; Guillot, R.; Yachandra, V. K.; Yano, J.; Neese, F.; Anxolabéhère-Mallart, E. Activation of a water molecule using a mononuclear Mn complex: from Mn-aquo, to Mn-hydroxo, to Mn-oxyl via charge compensation. *Energy Environ. Sci.* **2010**, *3*, 924–938.